ACS APPLIED MATERIALS & INTERFACES

Research Article

www.acsami.org

Blue and Blue-Green Light-Emitting Cationic Iridium Complexes: Synthesis, Characterization, and Optoelectronic Properties

Chozhidakath Damodharan Sunesh,[†] Kanagaraj Shanmugasundaram,[†] Madayanad Suresh Subeesh,[†] Ramesh Kumar Chitumalla,[‡] Joonkyung Jang,[‡] and Youngson Choe*[,†]

[†]Department of Polymer Science and Chemical Engineering, Pusan National University, Busan 609-735, South Korea

[‡]Department of Nanomaterials Engineering, Pusan National University, Busan, 609-735, Republic of Korea

Supporting Information

ABSTRACT: Two new cationic iridium complexes, $[Ir(ppy)_2(phpzpy)]PF_6$ (complex 1) and $[Ir(dfppy)_2(phpzpy)]PF_6$ (complex 2), bearing a 2-(3-phenyl-1*H*-pyrazol-1-yl)-pyridine (phpzpy) ancillary ligand and either 2-phenylpyridine (Hppy) or 2-(2,4-difluorophenyl)pyridine (Hdfppy) cyclometalating ligands, were synthesized and fully characterized. The photophysical and electrochemical properties of these complexes were investigated by means of UV−visible spectroscopy, emission spectroscopy, and cyclic voltammetry. Density functional theory (DFT) and time dependent DFT (TD-DFT) calculations were performed to simulate and study the photophysical and electrochemical properties of both complexes. Light-emitting electrochemical cells (LECs) were fabricated by incorporating complexes 1 and 2, which respectively exhibit blue-green (488 and 516 nm) and blue (463 and 491 nm) emission colors, achieved through the meticulous design of the ancillary ligand. The luminance and current efficiency measurements recorded for the LEC based on complex 1 were 1246 cd m^{-2} and 0.46 cd A^{-1}, respectively, and were higher than those measured for complex 2 because of the superior balanced carrier injection and recombination properties of the former.

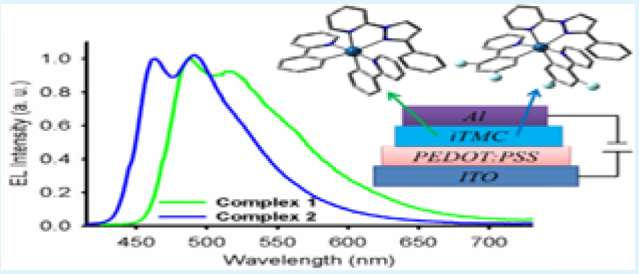

KEYWORDS: *light-emitting electrochemical cells, iridium complexes, pyrazole, thin film, electroluminescence*

1. INTRODUCTION

As state-of-the-art solid-state lighting devices, light-emitting electrochemical cells (LECs) have aroused widespread attention due to their simple device structure and low-cost production.[1−5] In contrast with conventional organic light-emitting diodes (OLEDs), of which the active layer consists of an emitting material with a neutral charge, the active layer of LECs contains ionic species. The active layer is deposited by a solution process via spin coating and its mobile ions drift toward the respective electrodes under an external bias and execute the process of electroluminescence (EL) through charge injection, transportation, and emissive recombination, a process which is quite different from that of OLED. Moreover, the migrant ions in the active layer allow LECs to use air-stable electrodes, permitting the nonrigorous encapsulation of the devices, which enables them to function under application of a low operating voltage.[3−5] With the aforementioned advantages, LECs have emerged as promising candidates for next generation display and lighting applications ahead of sophisticated OLEDs. OLEDs, which consist of a multilayered stack structure deposited by multiple vacuum sublimation processes, require rigorous encapsulation, which increases their manufacturing cost to an extent that it prevents the technology from penetrating the lighting industry.

The luminescent materials used in LECs generally consist of conjugated polymers or ionic transition metal complexes (iTMCs). The concept of an LEC was first proposed by Heeger in 1995, who used an emissive conjugated polymer, along with an ion conducting polymer, and an inorganic salt.[1] Thereafter, in 1996, an LEC utilizing iTMCs, which employed an ionic ruthenium complex containing a 4,7-diphenyl-1,10-phenanthroline ligand bearing charged sulfonate groups on the para position of the phenyl groups was reported.[6] Subsequently, LECs based on iTMCs have attracted significant attention after their phosphorescent nature became known. Compared to polymer-based LECs, iTMC-LECs have a simple composition, because they require neither an ion-conducting polymer nor an inorganic salt for charge injection purposes.[2,3,6−12] The use of a single component as a light-emitting material avoids the undesired aggregation or phase separation associated with polymer LECs, thereby resulting in a smooth film morphology for improved device performance. An essential advantage of iTMCs is their processability, that is, their solubility in most polar solvents, which allows these materials to be applied to large areas by the spin coating process. Moreover, iTMCs

Received: January 29, 2015
Accepted: March 19, 2015
Published: March 19, 2015

DOI: 10.1021/acsami.5b00875
ACS Appl. Mater. Interfaces 2015, 7, 7741−7751

possess good thermal and photochemical stabilities and, in addition, they exhibit exceptional phosphorescent quantum yields. Furthermore, high luminance efficiency is customary for LECs based on iTMCs by virtue of their phosphorescent nature.

To date, the operational mechanisms proposed for LECs are the electrodynamical (ED)[13−15] and electrochemical doping (ECD)[1,16,17] models, of which iTMC-based LECs follow the former model because of their intrinsic ionic nature. The ED model assumes that the mobile ions in the active layer are transported and accumulate at the respective electrodes under the application of an external bias to form an electrical double layer, which generates strong interfacial electric fields at the electrode surfaces responsible for facilitating the injection of charge carriers. These charge carriers transport and recombine in the bulk, thereby resulting in the emission of light.

A large number of iTMCs were reported soon after the introduction of a Ru(II) complex for LEC applications.[18−24] The well-known phosphorescent emitters used in the early stages of LEC applications were based on ionic Ru(II)[6,18−24] and Os(II)[22,25] complexes. However, the low ligand−field splitting energies (LFSEs) of these complexes result in red or orange-red emissions, which limit their application in LEC devices. Furthermore, LECs based on these complexes exhibit low luminescent efficiencies. Thereafter, ionic Cu(I) complexes were utilized in LECs to take advantage of their low cost and low toxicity,[8−10,26] although the low LFSEs of these complexes impede their performance. Moreover, it is not possible to tune the emission colors of LECs employing these complexes in the short-wavelength region; thus, they are not good candidates for lighting applications. The utilization of cationic iridium complexes in lighting devices offered a tremendous improvement over other metal complexes, because of their higher LFSEs. The high LFSE of an iridium complex is a consequence of the large size and charge of the heavy iridium atom endowed by strong spin−orbit coupling.

The first LEC based on an ionic iridium complex was reported by Slinker et al. in 2004.[27] This LEC emitted yellow light and exhibited a peak brightness of 300 cdm^{-2} and a peak power efficiency exceeding 10 lm W^{1-} under 3 V.[27] Soon after this a wide variety of iridium complexes were reported, thereby exploiting the large LFSEs of these complexes.[2,11,12,26,28−33] The large LFSE of iridium complexes renders the dissociate e_g orbitals less accessible compared to those of Ru(II) complexes. These features enhance the photochemical stability and result in a high photoluminescent quantum yield (PLQY). An important peculiarity of an iridium complex is its versatility in terms of the adjustment of the emission colors through structural modification of its organic ligands. These features have since earned iridium complexes a prominent position in LEC research. However, for solid-state lighting applications, LECs emitting the colors blue, green, and red are very important, because of the scarcity of compounds with these properties. Apart from this, the combination of these primary colors to produce white is a prerequisite for display and lighting applications.[34]

This paper proposes a new strategy to shift the emission color of cationic iridium complexes to the blue region of the visible spectrum by using a new ancillary ligand, 2-(3-phenyl-1*H*-pyrazol-1-yl)pyridine (phpzpy), which was synthesized by a noncatalyzed C−N coupling reaction in the presence of a base.[35] The corresponding heteroleptic cationic iridium complexes, $[Ir(ppy)_2(phpzpy)]PF_6$ (complex 1) and $[Ir(dfppy)_2(phpzpy)]PF_6$ (complex 2) were synthesized from the Hppy (2-phenylpyridine) and Hdfppy (2-(2,4-difluorophenyl)pyridine cyclometalating ligands using previously reported procedures.[36,37] The synthesis, structural, photophysical, and electrochemical properties of the complexes are presented in detail. Density functional theory (DFT) and time dependent DFT (TD-DFT) calculations are simulated for both complexes, and the results are corroborated with the photophysical and electrochemical behavior. Both of the new complexes were incorporated to fabricate LEC devices to enable an investigation of their electroluminescent properties.

2. EXPERIMENTAL SECTION

2.1. Materials and Methods. Apart from iridium(III) chloride hydrate, 99.9% ($IrCl_3 \cdot xH_2O$), all other reactants and solvents were purchased from Sigma-Aldrich, South Korea, whereas the former material was purchased from Alfa Aesar and used without further purification. ^1H and ^{13}C NMR spectra were recorded on a Varian Unity Inova 500 MHz FT-NMR spectrometer. Chemical shifts δ (in ppm) were measured relative to the residual CD_2Cl_2 solvent peak with tetramethylsilane as an internal standard. Elemental analyses were performed on an Elementar Vario EL CHN elemental analyzer. Mass spectra were recorded on an Agilent, Q-TOF 6530 MS/MS system. The UV−visible absorption spectra and photoluminescence (PL) emission spectra of the complexes were recorded in a 1 cm path-length quartz cell using an Agilent 8453 spectrophotometer and an F−7000 FL spectrophotometer, respectively. The PLQYs were measured in acetonitrile solutions at an excitation wavelength of 395 nm with quinine bisulfate (Φp = 0.545 in 1 M H_2SO_4) as the reference substance. The surface morphology of the films was investigated using atomic force microscopy (AFM). Electrochemical measurements of the complexes were performed using cyclic voltammetry and recorded using a potentiostat/galvanostat (Iviumstat) voltametric analyzer in acetonitrile solutions (10^{-3} M) with a scan rate 100 mVs^{-1}. The electrolytic cell consists of glassy carbon as the working electrode, platinum wire as the counter electrode, and Ag/AgCl as the reference electrode. The supporting electrolyte was 0.1 M solution of tetrabutylammonium hexafluorophosphate ($TBAPF_6$) in acetonitrile. The redox potentials of each measurement were recorded against the ferrocenium/ferrocene (Fc^+/Fc) couple that was used as an internal standard. The HOMO/LUMO energy levels and the energy gap (E_{gap}) of the complexes were calculated from the oxidation (E_{ox}) and reduction (E_{red}) potentials using the empirical relations:[38,39] $E_{HOMO} = [-e(E_{ox(vsAg/AgCl)} - E_{1/2(Fc/Fc+vsAg/AgCl))}] - 4.8$ eV; $E_{LUMO} = [-e(E_{red} - E_{1/2})] - 4.8$ eV, and $E_{gap} = E_{HOMO} - E_{LUMO}$, where $E_{1/2(Fc/Fc+vsAg/AgCl)}$ is the redox potential of ferrocene, which was found to be 0.43 V. E_{HOMO} and E_{LUMO} are the energy levels of the highest occupied and lowest unoccupied molecular orbitals, respectively.

2.2. Synthesis of 2-(3-Phenyl-1*H*-pyrazol-1-yl)pyridine (phpzpy). The ancillary ligand, phpzpy, was synthesized by using the reported procedure, which involves a noncatalyzed C−N coupling reaction in the presence of base.[35] 3-Phenyl-1*H*-pyrazole and potassium *tert*-butoxide were dissolved at room temperature in dry DMSO (5 mL). To the basic solution, 2-bromopyridine was added slowly under constant stirring. The reaction mixture was refluxed at 140 °C for 12 h under nitrogen and then cooled to room temperature, after which it was extracted with water and ether. The organic layer was washed with water and ether to remove DMSO as well as excess potassium *tert*-butoxide. The organic layer was then isolated, dried over anhydrous Na_2SO_4, and filtered. The solvent was then removed under reduced pressure. The crude product was purified by column chromatography on silica gel (200−300 mesh) with hexane/ethyl acetate (9:1) as the eluent, to yield colorless oil that crystallized into colorless solid crystals after a while. ^1H NMR (500 MHz, CD_2Cl_2) δ (ppm): 8.59 (d, J = 8.29 Hz, 1H), 8.41 (d, J = 4.73 Hz, 1H), 8.10 (d, J = 8.29 Hz, 1H), 7.92 (d, J = 7.67 Hz, 2H), 7.82 (t, J = 7.81 and 7.81 Hz, 2H), 7.43 (t, J = 7.48 and 7.48 Hz, 1H), 7.34 (t, J = 7.32 and 7.32 Hz, 1H), 7.21 (t, J = 7.41 and 7.41 Hz, 1H), 6.78 (d, J = 2.51 Hz, 1H).

DOI: 10.1021/acsami.5b00875
ACS Appl. Mater. Interfaces 2015, 7, 7741−7751

Scheme 1. Synthetic Routes and Structures of the Cationic Iridium Complexes[a]

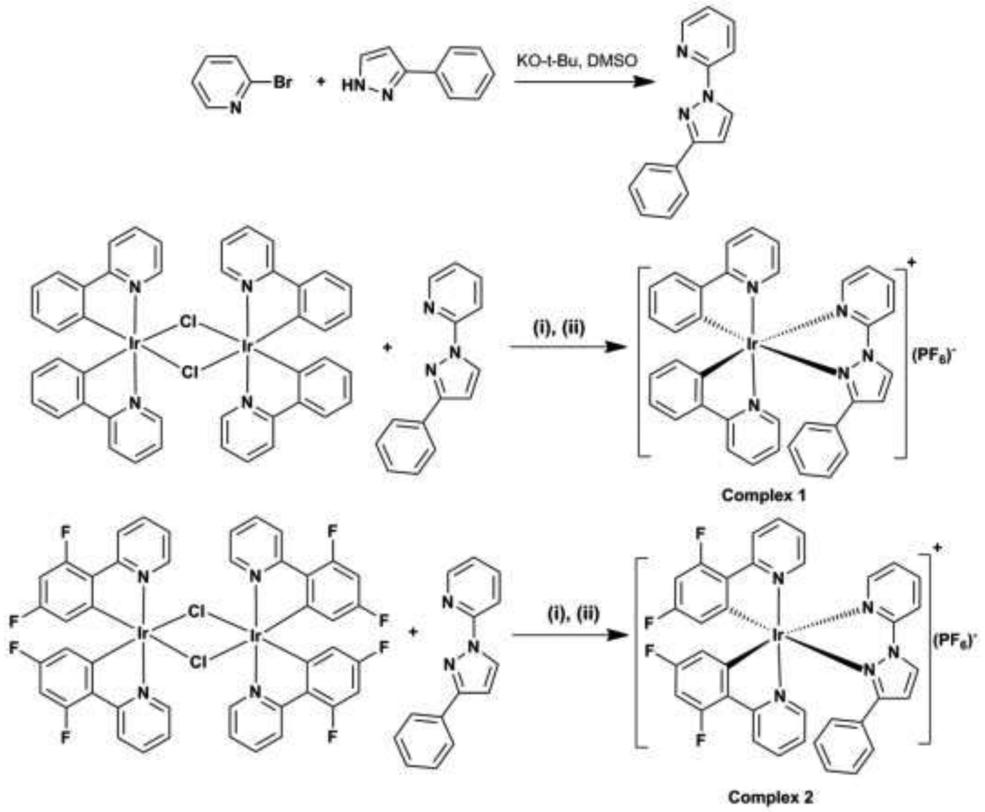

[a]Conditions: (i) 1,2-ethanediol (15 mL), 150°C for 16 h; (ii) NH_4PF_6 (1 g in 10 mL water), 1 h.

2.3. Synthesis of $[Ir(ppy)_2(phpzpy)]PF_6$ (Complex 1). The cyclometalated dichloro-bridged dimeric iridium $[Ir(ppy)_2Cl]_2$ (108 mg, 0.1 mmol) and neutral pyrazole-based ancillary ligand, phpzpy (51 mg, 0.23 mmol), were dissolved in 1,2-ethanediol (15 mL). The reaction mixture was heated to reflux at 150 °C for 16 h under nitrogen atmosphere with constant stirring and then cooled to room temperature. A concentrated solution of NH_4PF_6 (1 g, 6.13 mmol) in deionized water (10 mL) was added slowly to the reaction mixture under stirring for 1 h, resulting in a yellow suspension. The suspension was filtered and the resultant precipitate was washed with plenty of deionized water. The yellow precipitate obtained was dried under vacuum at 100 °C for 12 h. The crude material was subsequently crystallized from dichloromethane/hexane, yielding a yellow powder. Yield: 139 mg, 0.16 mmol, 80%. ^{1}H NMR (500 MHz, CD_2Cl_2) δ (ppm): 8.71 (d, J = 3.05 Hz, 2H), 8.32 (d, J= 5.47 Hz, 1 H), 8.18 (d, J = 1.57 Hz, 2H), 8.16−8.10 (m, 2H), 7.95−7.90 (m, 2H), 7.83 (d, J = 1.11 Hz, 1H), 7.81−7.78 (m, 2H), 7.72−7.62 (m, 4H), 7.30 (d, J = 7.84 Hz, 2H), 7.27−7.24 (m, 2H), 7.07−6.99 (m, 3H), 6.88−6.81 (m, 4H). ^{13}C NMR (126 MHz, CD_2Cl_2) δ (ppm): 160.19, 149.99, 149.23, 148.22, 146.88, 144.01, 143.82, 141.91, 138.74, 133.14, 132.04, 131.51, 131.14, 130.24, 129.69, 128.42, 128.14, 125.24, 125.04, 124.01, 123.32, 122.38, 120.33, 119.88, 113.50, 112.58. ESI-MS (m/z): 722.2 $[M - PF_6]^+$. Anal. Calcd (%) for $C_{36}H_{27}N_5PF_6Ir$: C 49.88, H 3.14, N 8.08; Found: C 49.82, H 3.18, N 8.13.

2.4. Synthesis of $[Ir(dfppy)_2(phpzpy)]PF_6$ (Complex 2). Complex 2 was synthesized by reacting $[Ir(dfppy)_2Cl]_2$ (122 mg, 0.1 mmol) and phpzpy (51 mg, 0.23 mmol) in 1,2-ethanediol (15 mL) under nitrogen followed by ion exchange to replace Cl^- with PF_6^-. Yield: 164 mg, 0.17 mmol, 87%. ^{1}H NMR (500 MHz, CD_2Cl_2) δ (ppm): 8.74 (d, J = 3.3 Hz, 2H), 8.33 (d, J = 5.60 Hz, 1 H), 7.99 (d, J = 4.99 Hz, 2H), 7.90−7.85 (m, 1H), 7.71 (d, J = 5.34 Hz, 2H), 7.64−7.60 (m, 3H), 7.35−7.31 (m, 2H), 7.23−7.17 (m, 2H), 7.11−7.01 (m, 3H), 6.88−6.83 (m, 4H), 6.80 (d, J = 3.01 Hz, 1H). ^{13}C NMR (126 MHz, CD_2Cl_2) δ (ppm): 165.33, 164.98, 162.28, 160.40, 151.63, 149.42, 148.87, 148.02, 142.71, 139.73, 138.31, 133.88, 130.28, 128.63, 128.062, 125.39, 124.38, 123.38, 114.08, 112.89. Anal. Calcd (%) for $C_{36}H_{27}N_5PF_6Ir$: C 49.88, H 3.14, N 8.08; Found: C 49.75, H 3.19, N 8.19. ESI-MS (m/z): 794.1 $[M - PF_6]^+$. Anal. Calcd (%) for $C_{36}H_{23}N_5PF_{10}Ir$: C 46.06, H 2.47, N 7.46; Found: C 46.13, H 2.43, N 7.52.

2.5. Fabrication and Characterization of LEC Devices. The buffer layer material, poly(3,4-ethylenedioxythiophene)/poly styrenesulfonate (PEDOT:PSS) was purchased from H. C. Starck (Clevios AI 4083) and used as the hole conducting material. Indium tin oxide (ITO) coated glass plates, patterned using conventional photolithography, were purchased from Samsung Corning, South Korea. Prior to the fabrication process, the ITO glass plates were extensively cleaned by sonication in a solvent mixture consisting of ethanol, acetone, and isopropyl alcohol (1:1 v/v) for 30 min followed by UV−ozone treatment for 30 min.

The LEC devices were fabricated as follows. Primarily, the PEDOT:PSS solution was spin coated at 2000 rpm for 20 s onto the precleaned ITO surfaces to give film thickness of 50 nm and baked at 120 °C for 10 min. Prior to the spin coating procedure, PEDOT:PSS was filtered using a 0.2 μm hydrophilic PTFE−filter. The PEDOT:PSS is used as a buffer layer with the purpose of increasing the yield and reproducibility of the LEC devices. The active layer solution was then spin coated at 2000 rpm for 20 s onto the ITO/PEDOT:PSS layer and baked at 70 °C for 1 h in a vacuum oven. The active layer solution was prepared from 20 mg of the complex in 1 mL of acetonitrile solution. Before spin coating, the active layer solution was maintained inside the shaking incubator for 24 h and then filtered using a 0.1 μm hydrophobic PTFE−filter. The substrate containing the spin-coated active layer (75 nm) was then transferred into a metal-evaporating chamber, for deposition of the aluminum (100 nm) cathode using a shadow mask under high vacuum. The layer structure of the resulting devices had the configuration ITO/PEDOT:PSS/iTMCs/Al. The light-emitting area of the device was 4

DOI: 10.1021/acsami.5b00875
ACS Appl. Mater. Interfaces 2015, 7, 7741−7751

mm × 5 mm. The electroluminescent properties of these devices were evaluated using Keithley characterization systems in ambient conditions. The current density and luminance versus voltage sweeps were measured using a Keithley 2400 source meter and calibrated with a silicon photodiode. An Avantes luminance spectrometer was used to measure the EL spectrum and Commission Internationale de L'Eclairage (CIE) coordinates.

3. RESULTS AND DISCUSSION

3.1. Synthesis and Characterization. The ancillary ligand, phpzpy, was synthesized in dry DMSO solution by combining 3-phenyl-1*H*-pyrazole and 2-bromopyridine using a noncatalyzed C−N coupling reaction in the presence of potassium *tert*-butoxide as a base.[35] The targeted iridium complexes were synthesized in two steps. The first step involved the synthesis of the cyclometalated Ir^{III} μ-dichloro bridged dimer, $[Ir(C\wedge N)_2(\mu\text{-}Cl)]_2$ starting from $IrCl_3{\cdot}xH_2O$ with 2.5 equiv of the required cyclometalating ligands (C∧N), namely, 2-phenylpyridine (Hppy) or 2-(2,4-difluorophenyl)-pyridine (Hdfppy) in a 2-ethoxyethanol/water mixture (3:1, 40 mL).[40] The second step involved the facile reaction of the dimeric Ir(III) intermediates with the neutral phpzpy ancillary ligand to form the cationic iridium complexes as chloride salts. Subsequently, the chloride complexes were subjected to an ion exchange reaction to replace Cl^- with PF_6^- using ammonium hexafluorophosphate (NH_4PF_6) to produce the cationic iridium complexes in high yields. These iridium complexes were characterized by various spectroscopic, photophysical, electrochemical, and computational methods. The synthetic routes showing the structures of the ancillary ligand and cationic iridium complexes are depicted in Scheme 1.

3.2. Photophysical Properties. The UV−visible absorption spectra of the complexes were recorded at room temperature in acetonitrile solutions and are shown in Figure 1. The absorption spectra show intense absorption bands below

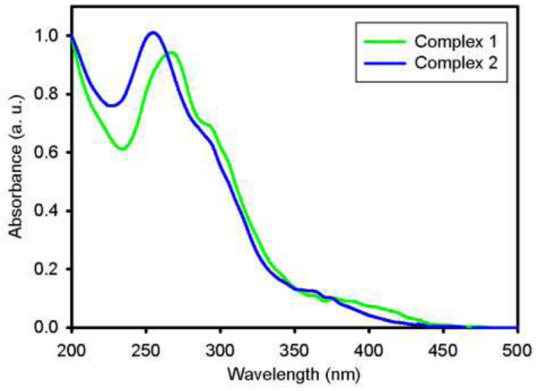

Figure 1. UV−visible absorption spectra of the cationic iridium complexes in acetonitrile solutions at room temperature.

340 nm, which are assigned to the spin-allowed ligand-centered (LC) $^1\pi-\pi^*$ transitions of the coordinated cyclometalating and ancillary ligands. These LC bands are accompanied by less intense absorption bands, which are observed from 350 nm and extend toward the visible region. These lower energy absorption bands are ascribed to the spin-allowed metal-to-ligand charge-transfer (^{1}MLCT), spin-forbidden metal-to-ligand charge-transfer (^{3}MLCT), ligand-to-ligand charge-transfer (^{3}LLCT and ^{1}LLCT), and ligand-centered (LC) $^3\pi-\pi^*$ transitions of the complexes.[7] The spin-forbidden transitions, such as ^{3}MLCT, ^{3}LLCT, and ^{3}LC, gain substantial intensity by mixing with higher lying ^{1}MLCT transitions owing to the strong spin−orbit coupling of the heavy iridium atom.[37,41] The observed blue shift of 28 nm of the absorption spectrum of complex 2 relative to that of complex 1 is ascribed to the electron-withdrawing fluorine atoms on the cyclometalated ligands of the former complex. The main absorption bands and their molar extinction coefficients of complex 1 and complex 2 are given in Table 1, and the values are fully consistent with the results of the quantum chemical calculations (section 3.4).

Figure 2 shows the room-temperature PL emission spectra of the complexes in acetonitrile solutions in which the complexes show broad and structured emission peaks upon excitation. These vibronically structured emission spectra indicate that the emissive excited states have a predominantly LC $^3\pi-\pi^*$ character in addition to ^{3}MLCT character.[32,37,41] The photophysical properties of complexes 1 and 2 are summarized in Table 1. In acetonitrile solution, complex 1 emits blue-green light with peak and shoulder emissions at 489 and 508 nm, respectively. However, the emission spectrum of complex 2 displays a marked shift toward the blue wavelength region relative to complex 1 with a peak emission at 465 nm and a shoulder peak at 484 nm. The hypsochromic shift in the emission spectrum of complex 2 is accomplished by the significant stabilization of the HOMO as a consequence of the electron-withdrawing fluorine atoms on the cyclometalated ligands of this complex. Furthermore, the PLQYs of the complexes were also measured in degassed acetonitrile solutions and showed high values of 0.17 and 0.14 for complexes 1 and 2, respectively. These PLQY values are comparable irrespective of the distinctive photophysical behavior of complexes 1 and 2.

The PL emission spectra of neat films of the complexes (see Figure S1 in the Supporting Information) resemble the emission spectra in solution with vibronically structured peaks displaying maximum at 484 nm and a lower intensity shoulder at 514 nm for complex 1, whereas those of complex 2 occur at 463 and 489 nm, respectively. Compared with the PL emission spectra of the solutions, the bands of the PL spectra of the neat films of the complexes are broadened with long tails extending to 700 nm and red-shifted by 5−6 nm. These features of the PL spectra of the neat films are indicative of strong intermolecular interactions. The PLQYs of neat films of complexes 1 and 2 are shown in Table 1, which are lower than solution PLQYs owing to the severe excited-state quenching in neat films.

3.3. Electrochemical Properties. The electrochemical behavior of the complexes was investigated by cyclic voltammetry (CV) and the redox potentials were measured versus ferrocenium/ferrocene (Fc^+/Fc) using 0.1 M $TBAPF_6$ in acetonitrile. The measured redox potentials are summarized in Table 1. Figure 3 displays the cyclic voltammograms of the complexes, which demonstrate reversible oxidation and irreversible reduction waves in acetonitrile solution. During the anodic scan, the complexes exhibited reversible oxidation waves at 1.32 and 1.66 V for complexes 1 and 2, respectively. These anodic waves are accredited to the oxidation of Ir(III) to Ir(IV) with a substantial contribution from the cyclometalated ligand. The oxidation potential of complex 2 is anodically shifted by 340 mV compared to that of complex 1. This indicates the stabilization of the HOMO of complex 2 owing to the electron-withdrawing fluorine atoms, which reduces the electron density around the iridium center. Similarly, in the cathodic scan, the complexes display irreversible reduction

DOI: 10.1021/acsami.5b00875
ACS Appl. Mater. Interfaces 2015, 7, 7741−7751

Table 1. Photophysical and Electrochemical Properties of Cationic Iridium Complexes

			emission at room temperature λ_{em} [nm]				electrochemical data[e]		
complex	λ_{abs}[a] [nm] (ε [$\times 10^4$ M^{-1} cm^{-1}])	PL excitation wavelength λ_{max} [nm]	solution[b]	film[c]	Φ_{em}[d] solution	Φ_{em}[d] film	E_{ox} [V]	E_{red} [V]	E_{gap} [eV]
1	267 (2.81), 292 (2.04), 364 (0.33), 379 (0.30), 391 (0.27), 419 (0.17)	420	489, 508 sh	484, 514 sh	0.17	0.13	1.32	−2.01	3.33
2	255 (2.88), 290 (1.89), 344 (0.46), 365 (0.37), 374 (0.31), 391 (0.19)	390	465, 484 sh	463, 489 sh	0.14	0.10	1.66	−1.98	3.64

[a]Measured in acetonitrile solution at 1.0×10^{-5} M concentration. [b]Maximum emission wavelength, measured in acetonitrile solution at 1.0×10^{-5} M; the symbol sh denotes the shoulder wavelength. [c]Maximum emission wavelength, measured in film state. [d]PL quantum yield of solution and neat films measured versus quinine bisulfate in 1N H_2SO_4. [e]Electrochemical data versus Fc^+/Fc (Fc is ferrocene) measured in 1.0×10^{-3} M acetonitrile solution

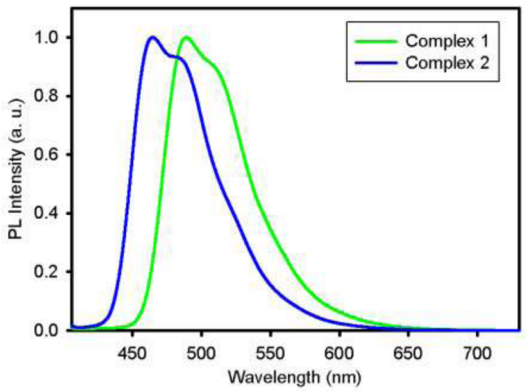

Figure 2. Photoluminescence (PL) emission spectra of cationic iridium complexes in acetonitrile solutions at room temperature.

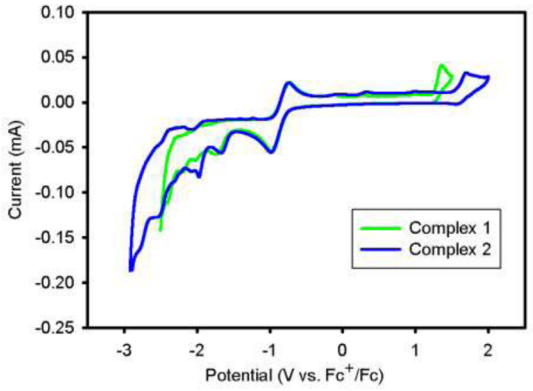

Figure 3. Cyclic voltammograms of the complexes in acetonitrile solution (10^{-3} M). The potentials were recorded versus Fc^+/Fc (ferrocene).

peaks at −2.01 V for complex 1 and −1.98 V for complex 2. The reduction potentials of the complexes correspond to the energy of the LUMO (see section 3.4), which is considered to be caused by the ancillary ligand with only a partial contribution from the metal center. The fact that similar reduction potentials were measured for both complexes 1 and 2, confirms that the ancillary ligand, which is present in both of these complexes, is responsible for the reduction. The HOMO and LUMO energies of the complexes were calculated from the oxidation and reduction potentials using the empirical relations.[38,39] The calculated HOMO energies are −5.69 and −6.03 eV for complexes 1 and 2, respectively, while the LUMO energies are −2.36 and −2.39 eV, respectively. The electrochemical energy gaps ($E_{gap} = E_{HOMO} - E_{LUMO}$) of complexes 1 and 2 are 3.33 and 3.64 eV, respectively. The higher energy gap of complex 2 results from the electron-withdrawing fluorine atoms, followed by significant HOMO stabilization compared to complex 1.

3.4. Quantum Chemical Calculations. DFT studies of the two cationic iridium(III) complexes were carried out using Gaussian 09 (revision B.01) ab initio quantum chemical program.[42] Geometry optimization and the vibrational frequency analysis of the complexes were performed by employing a hybrid Becke,[43,44] three-parameter, Lee−Yang−Parr[45] exchange−correlation functional (B3LYP). We used 6-31G(d,p) basis functions for the H, C, N, and F atoms. In addition, a "'double-ξ'" quality basis set consisting of Hay and Wadt's effective core potentials (LanL2DZ ECP)[46−48] was used for the iridium atom. No symmetry constraints were applied during the geometry optimizations. We performed a vibrational frequency analysis to confirm that each configuration is indeed a minimum on the potential energy surface.

On the basis of the optimized structures of the electronic ground state, the absorption spectra of the two complexes were obtained in acetonitrile solution by using the TD-DFT method. The phosphorescence emission data were obtained by using the ΔSCF method. We used a self-consistent reaction field (SCRF) theory, referred to as the integral equation formalism polarizable continuum model (IEF-PCM)[49,50] to account for the solvation of the complexes. The TDDFT calculations were performed by using the B3LYP functional and the mixed basis set as described above. This combination of the theory and basis set has been successfully applied to studies of ruthenium complexes.[51]

The DFT/TDDFT calculations were performed for complexes 1 and 2 to examine their structural, electronic, and photophysical properties. Both complexes have a pseudo-octahedral coordination geometry around the metal center. The optimized geometries of the two complexes are shown in Figure 4, along with the geometrical parameters around the metal center. The bond lengths between the cyclometalated ligands and Ir (Ir−N/Ir−C) are approximately 2.01 Å. For the ancillary ligands, the corresponding distances are slightly longer, ranging from 2.2 to 2.3 Å. The bond angles of the cyclometalated phenylpyridine and ancillary ligands with Ir were found to be approximately 80° and 74°, respectively. These geometrical parameters are not significantly altered upon replacement of two of the hydrogen atoms with fluorine substituents on each of the two cyclometalated phenylpyridines of complex 1 (to give complex 2).

The Kohn−Sham orbitals (isosurface = 0.02 e $Å^{-3}$) of the complexes are displayed in Figure 5. The HOMO and HOMO

DOI: 10.1021/acsami.5b00875
ACS Appl. Mater. Interfaces 2015, 7, 7741−7751

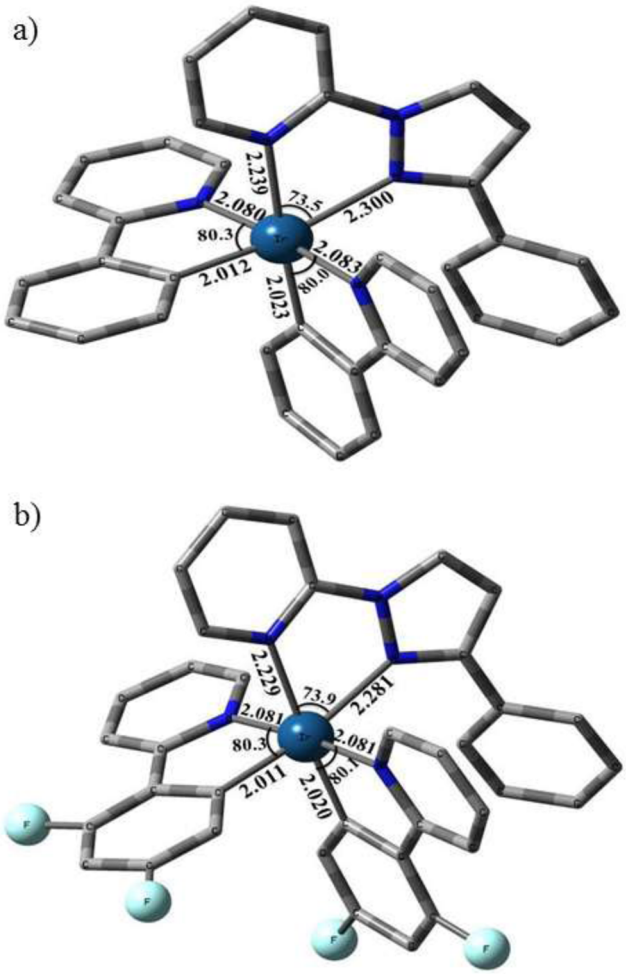

Figure 4. Optimized molecular structures of complexes 1 (a) and 2 (b). The hydrogen atoms are omitted here for clarity. Bond distances and angles are in units of Å and degrees, respectively.

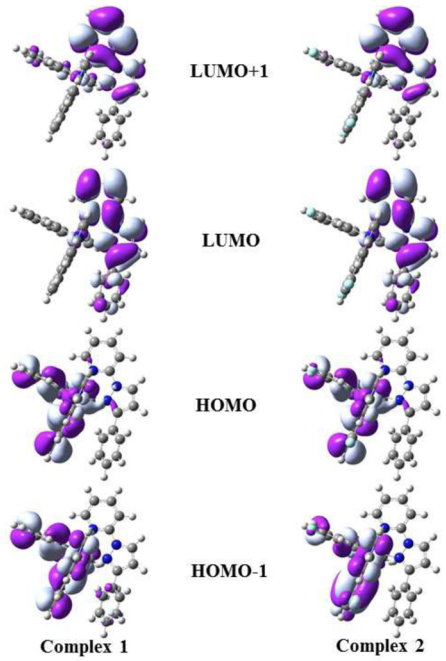

Figure 5. Electron density contours calculated for the HOMO − 1 to the LUMO + 1 of complexes 1 and 2 (isosurface = 0.02 e Å^{-3}).

− 1 are mainly localized on the metal and the two cyclometalated ligands, whereas the LUMO and LUMO + 1 are localized over the ancillary ligand. As the HOMO is delocalized across the cyclometalated ligands, any substitution on these ligands could be expected to affect the HOMO energy to a larger extent than the LUMO energy. Therefore, the HOMO is stabilized by the presence of the electron-withdrawing fluorine substituents on the cyclometalated ligands. The HOMO is stabilized by 0.31 eV, varying from −5.68 (complex 1) to −5.99 eV (complex 2). This stabilization of the HOMO explains the higher oxidation potential that was measured for complex 2 (1.66 V), compared to that of complex 1 (1.32 V). On the other hand, the LUMO is stabilized by only 0.08 eV, changing from −2.02 (complex 1) to −2.10 eV (complex 2). As a result, the HOMO−LUMO gap (HLG) of complex 2 (3.89 eV) is found to be 0.23 eV larger that of complex 1 (3.66 eV). The HOMO and LUMO energies and the HLG values from the present calculations are in perfect agreement with the electrochemical data inferred from the CV measurements. Noticeable hypsochromic shifts in the absorption and emission spectra are therefore expected in the transition from complex 1 to complex 2. The percentage distributions of the HOMO and LUMO are given in Table 2 for both complexes. The HOMO is largely located on the Ir (∼45%) and the cyclometalated ligands (∼50%), whereas the LUMO is largely located on the ancillary ligand (∼94%).

Table 2. Percentage Distribution of HOMO and LUMO in Complexes 1 and 2

	complex 1		complex 2	
	HOMO	LUMO	HOMO	LUMO
Ir	46.3	2.9	43.8	3.0
cyclometalated ligands	50.3	3.1	52.8	3.4
ancillary ligand	3.4	94.0	3.4	93.5

The UV−visible absorption spectra of the complexes were simulated in acetonitrile solution and are depicted in Figure 6 where it can be seen that the TD-DFT simulation reproduced the main bands observed in the experimental UV−visible spectrum. Theoretically obtained absorption maxima of complex 1 and 2 in the low energy region are located at 397 and 371 nm, respectively. The observed absorption arises from the transition of the HOMO to the LUMO + 1 in both cases. The hypsochromic shift of 26 nm found for complex 2 is ascribed to the increased HLG upon fluorine substitution on the cyclometalated ligands (vide supra). Table 3 reports the calculated excitation wavelengths with the largest oscillator strengths and coefficient of configuration interaction together with the dominant contribution to each transition for complexes 1 and 2. The phosphorescence emission maxima obtained from the ΔSCF method are 531 and 507 nm for complexes 1 and 2, respectively, which are in excellent agreement with the experimental data. We found both the absorption and emission spectra of complex 2 blue-shifted by approximately 25 nm relative to those of complex 1. Spin density plots of the T_1 states for complexes 1 and 2 in acetonitrile were constructed and are depicted in Figure 7. From the plots, it can be observed that the excited state (T_1) of the complex 1 becomes localized on the Ir atom and one of the cyclometalated ligands as has been seen previously in other

DOI: 10.1021/acsami.5b00875
ACS Appl. Mater. Interfaces 2015, 7, 7741−7751

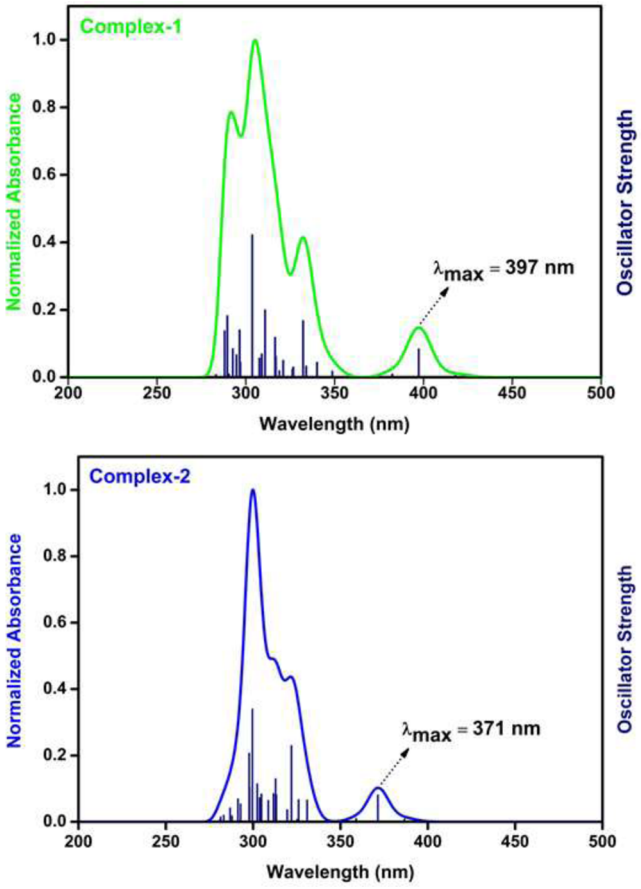

Figure 6. Simulated absorption spectra of the complexes 1 (top) and 2 (bottom). The vertical bars represent the oscillator strengths, and the spectra are broadened by using the Gaussian convolution with fwhm = 1000 cm^{-1}.

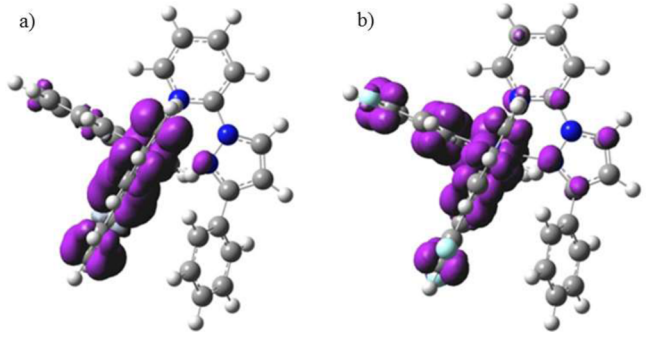

Figure 7. UB3LYP spin density contours of the unrestricted triplet state (T_1) (isocontour value = 0.002 e $Å^{-3}$) for (a) complexes 1 and (b) 2.

derivatives,[52,53] whereas the excited state (T_1) of the complex 2 becomes fully localized on the Ir atom, two cyclometalated ligands and also partly localized on the ancillary ligand.

3.5. Electroluminescent Properties of LECs. The potential practical application of the two cationic iridium complexes was explored by fabricating LECs with the device structure ITO/PEDOT:PSS//iTMC/Al, to which the PEDOT:PSS layer was added to smoothen the ITO surface.[32] To study the thin film surface morphologies of Complex 1 and Complex 2, AFM meseauremnts were performed. The films were prepared as the same method of fabrication process by spin coating the complexes 1 and 2 on the top of PEDOT:PSS/ITO layer. As shown in Figure 8, AFM images of complexes 1 and 2 shows smooth surface morphology and are pinhole free as the previously reported device.[54] The root−mean−square (rms) roughness of the films are 0.53 and 0.58 nm for the device based on complexes 1 and 2, respectively.

The EL spectra of the LECs incorporating the cationic iridium complexes are depicted in Figure 9. The EL spectra

Table 3. Calculated Excitation Wavelengths (λ_{cal}), Oscillator Strengths (f), and Coefficient of Configuration Interaction (CI) with Dominant Contribution to Each Transition for Complexes 1 and 2[a]

complex	transitions	λ_{cal} (nm)	f^b	CI coefficient	dominant contribution	$\lambda_{emission}$ (nm)
1	$S_0 \rightarrow S_1$	418	0.0056	0.6893	H → L (95%)	531
	$S_0 \rightarrow S_2$	**397**	**0.0844**	**0.6828**	**H → L + 1 (93%)**	
	$S_0 \rightarrow S_3$	382	0.0094	0.6941	H → L + 2 (96%)	
	$S_0 \rightarrow S_4$	349	0.0185	0.6947	H → L + 3 (97%)	
	$S_0 \rightarrow S_5$	340	0.0449	0.5390	H − 2 → L (58%)	
	$S_0 \rightarrow T_1$	453		0.5130	H → L + 1 (53%)	
	$S_0 \rightarrow T_2$	444		0.4636	H → L + 2 (43%)	
	$S_0 \rightarrow T_3$	421		0.6551	H → L (86%)	
	$S_0 \rightarrow T_4$	401		0.4679	H − 2 → L (44%)	
	$S_0 \rightarrow T_5$	385		0.3867	H → L + 1 (30%)	
2	$S_0 \rightarrow S_1$	387	0.0087	0.6782	H → L (92%)	507
	$S_0 \rightarrow S_2$	**371**	**0.0812**	**0.6696**	**H → L + 1 (90%)**	
	$S_0 \rightarrow S_3$	359	0.0099	0.6898	H → L + 2 (95%)	
	$S_0 \rightarrow S_4$	331	0.0660	0.5222	H − 1 → L (55%)	
	$S_0 \rightarrow S_5$	326	0.0672	0.4892	H → L + 3 (48%)	
	$S_0 \rightarrow T_1$	432		0.4617	H → L + 1 (43%)	
	$S_0 \rightarrow T_2$	428		0.4137	H → L + 2 (34%)	
	$S_0 \rightarrow T_3$	400		0.4173	H − 3 → L (35%)	
	$S_0 \rightarrow T_4$	387		0.5654	H → L (64%)	
	$S_0 \rightarrow T_5$	369		0.4244	H → L + 1 (36%)	

[a]The calculated emission values ($\lambda_{emission}$) from ΔSCF method. H and L denote HOMO and LUMO, respectively. [b]The oscillator strengths were given wherever applicable.

DOI: 10.1021/acsami.5b00875
ACS Appl. Mater. Interfaces 2015, 7, 7741−7751

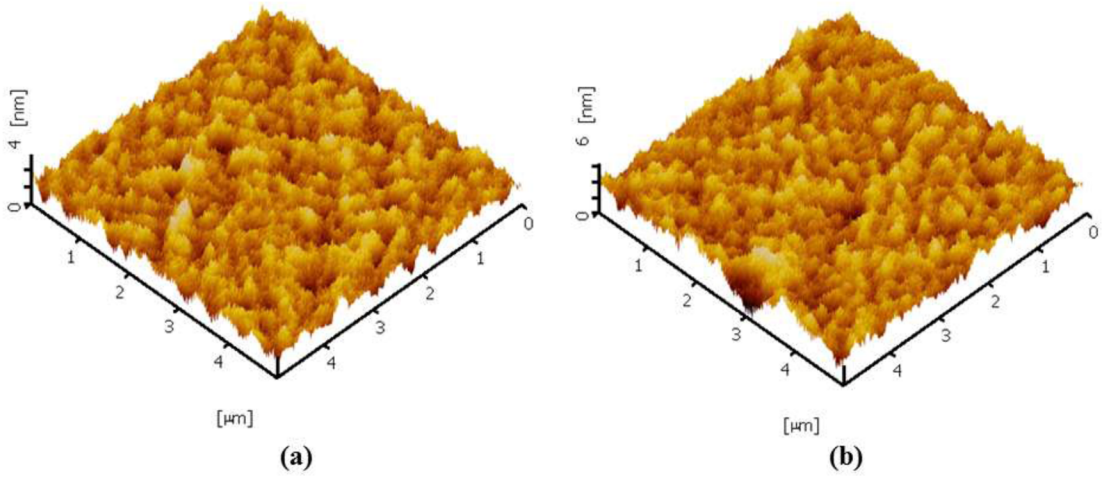

Figure 8. AFM images of thin films on the top of PEDOT:PSS/ITO layer: (a) complexes 1 and (b) 2.

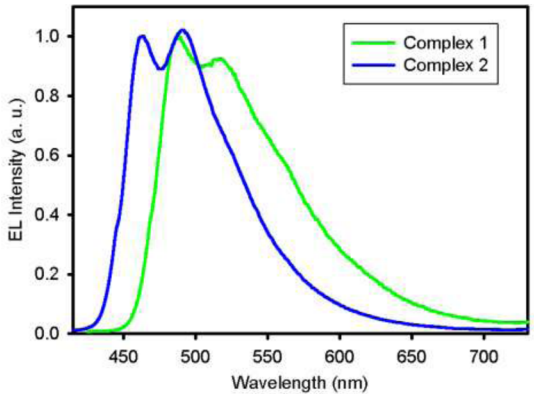

Figure 9. Electroluminescence (EL) spectra of LECs based on cationic iridium complexes.

resemble the PL spectra in acetonitrile in that they exhibit broad and structured emission peaks. The vibronically structured emission peaks indicate the prevalence of the same emission mechanisms in solution and the solid state, that is, light emission from the mixed ^{3}MLCT and ^{3}LC excited states. The LEC incorporating complex 1 displays a blue-green emission with an emission peak at 488 nm and a shoulder peak at 516 nm. However, the EL spectrum of complex 2 emits in the blue region, and shows an emission peak and a shoulder peak at 463 and 491 nm, respectively. Compared to complex 1, the EL spectrum of complex 2 is blue-shifted by 25 nm as a consequence of the influence of the electron-withdrawing fluorine atoms on the cyclometalating ligands. The CIE coordinates of LECs incorporating complexes 1 and 2 are (0.28, 0.50) and (0.24, 0.42), respectively. The EL spectra of LECs based on complexes 1 and 2 are comparable with the PL spectra of thin films of these complexes; however, the EL spectra are broadened compared to the PL spectra of the solutions and thin films. The considerable emission in the long-wavelength region of the EL spectra reflects the existence of strong intermolecular interaction in the films.

The voltage-dependent luminance and current density curves of LECs based on complexes 1 and 2 are shown in Figure 10. The device was scanned by using a single voltage scan with a sweep rate of 0.5 V/s. The devices incorporating the cationic iridium complexes exhibited a gradual increase in the luminance and current density with increasing voltage, a typical LEC

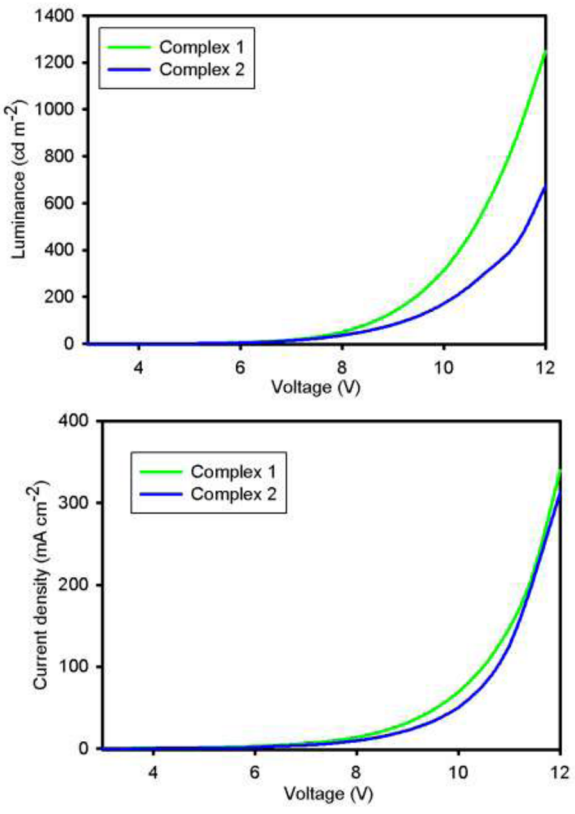

Figure 10. Luminance and current density versus voltage curves of LECs based on cationic iridium complexes.

characteristic, which occurs slowly at the starting bias, because of the slow migration of PF_6^- counter-anions toward the anode and the concurrent migration of the positively charged complex molecules to the cathode.[1,27,55] The intensity of the luminance and current density is almost constant up to 8 V and increases rapidly as the voltage is increased from 8 to 12 V. It is accomplished by the fast migration of mobile ions as the voltage increases, followed by increased carrier injection and recombination. The performance of LECs based on both complexes is summarized in Table 4. The LEC device based on complex 1 showed a maximum luminance of 1246 cd m^{-2} and current density of 339 mA cm^{-2} at 12 V, leading to a peak current efficiency of 0.46 cd A^{-1}. For complex 2, the

DOI: 10.1021/acsami.5b00875
ACS Appl. Mater. Interfaces 2015, 7, 7741−7751

Table 4. Electrical Characteristics of LECs Based on the Cationic Iridium Complexes

complex	luminance$_{max}$ [cd m^{-2}]	current density$_{max}$ [mA cm^{-2}]	current efficiency (cd A^{-1})	turn on voltage (V)	EL$_{max}$ (nm)	CIE coordinates
1	1246	339	0.46	4.0	488, 516	(0.28, 0.50)
2	674	312	0.38	4.5	463, 491	(0.24, 0.42)

performance of the LEC device is inferior in comparison, with a maximum luminance, current density, and current efficiency of 674 cd m^{-2}, 312 mA cm^{-2}, and 0.38 cd A^{-1}, respectively. The lower luminance and current efficiency of LECs based on complex 2 is caused by the enlarged energy gap, which would result in higher carrier injection barriers and a more unbalanced carrier recombination.

4. CONCLUSIONS

In conclusion, two new cationic iridium complexes containing 2-(3-phenyl-1*H*-pyrazol-1-yl)pyridine (phpzpy) ancillary ligand were synthesized and fully characterized. The photophysical and electrochemical properties of these complexes were studied and the results corroborated with the DFT/TD-DFT calculations. LECs were fabricated by utilizing complexes 1 and 2 and found to exhibit blue-green (488 and 516 nm) and blue (463 and 491 nm) electroluminescence with CIE color coordinates of (0.28, 0.50) and (0.24, 0.42) for complexes 1 and 2, respectively. Of these two complexes, LECs incorporating complex 1 resulted in a higher luminance of 1246 cd m^{-2} and a current efficiency of 0.46 cd A^{-1} compared to complex 2, owing to superior balanced carrier injection and recombination mechanisms. This work has therefore established that a pyrazole-based ancillary ligand is a promising component for tuning the emission color of iTMCs and that it could be used for solid-state lighting applications.

■ ASSOCIATED CONTENT

Ⓢ Supporting Information

PL emission spectra of neat films of the complexes. This material is available free of charge via the Internet at http://pubs.acs.org.

■ AUTHOR INFORMATION

Corresponding Author

*E-mail: choe@pusan.ac.kr. Tel.: +8251 510 2396. Fax: +8251 512 8634.

Notes

The authors declare no competing financial interest.

■ ACKNOWLEDGMENTS

This research was supported by Global Frontier Program through the Global Frontier Hybrid Interface Materials (GFHIM) of the National Research Foundation of Korea (NRF) funded by the Ministry of Science, ICT & Future Planning (2013M3A6B1078869) and the Brain Korea 21 Plus Project.

■ ABBREVIATIONS

LEC = Light-emitting electrochemical cell
iTMC = ionic transition metal complexes
LFSE = ligand-field splitting energies
phpzpy = 2-(3-phenyl-1*H*-pyrazol-1-yl)pyridine
CV = cyclic voltammetry
DFT = density functional theory
TD-DFT = time-dependent density functional theory
EL = electroluminescence
PL = photoluminescence
PEDOT:PSS = poly(3,4-ethylenedioxythiophene):poly styrenesulfonate
PLQY = photoluminescence quantum yield
SCF = spectral correlation function
SCRF = self-consistent reaction field
HOMO = highest occupied molecular orbital
LUMO = lowest occupied molecular orbital
HLG = HOMO−LUMO gap

■ REFERENCES

(1) Pei, Q.; Yu, G.; Zhang, C.; Yang, Y.; Heeger, A. J. Polymer Light-Emitting Electrochemical Cells. *Science* **1995**, *269*, 1086−1088.
(2) Sunesh, C. D.; Mathai, G.; Choe, Y. Constructive Effects of Long Alkyl Chains on the Electroluminescent Properties of Cationic Iridium Complex-based Light-Emitting Electrochemical Cells. *ACS Appl. Mater. Interfaces* **2014**, *6*, 17416−17425.
(3) Slinker, J.; Bernards, D.; Houston, P. L.; Abruna, H. D.; Bernhard, S.; Malliaras, G. G. Solid-State Electroluminescent Devices Based on Transition Metal Complexes. *Chem. Commun.* **2003**, *19*, 2392−2399.
(4) Slinker, J. D.; DeFranco, J. A.; Jaquith, M. J.; Silveira, W. R.; Zhong, Y.-W.; Moran-Mirabal, J. M.; Craighead, H. G.; Abruna, H. D.; Marohn, J. A.; Malliaras, G. G. Direct Measurement of the Electric-Field Distribution in a Light-Emitting Electrochemical Cell. *Nat. Mater.* **2007**, *6*, 894−899.
(5) Slinker, J. D.; Rivnay, J.; Moskowitz, J. S.; Parker, J. B.; Bernhard, S.; Abruna, H. D.; Malliaras, G. G. Electroluminescent Devices from Ionic Transition Metal Complexes. *J. Mater. Chem.* **2007**, *17*, 2976−2988.
(6) Lee, J. K.; Yoo, D. S.; Handy, E. S.; Rubner, M. F. Thin Film Light Emitting Devices from an Electroluminescent Ruthenium Complex. *Appl. Phys. Lett.* **1996**, *69*, 1686−1688.
(7) Lamansky, S.; Djurovich, P.; Murphy, D.; Abdel-Razzaq, F.; Lee, H.-E.; Adachi, C.; Burrows, P. E.; Forrest, S. R.; Thompson, M. E. Highly Phosphorescent Bis-Cyclometalated Iridium Complexes: Synthesis, Photophysical Characterization, and Use in Organic Light Emitting Diodes. *J. Am. Chem. Soc.* **2001**, *123*, 4304−4312.
(8) Wang, Y.-M.; Teng, F.; Hou, Y.-B.; Xu, Z.; Wang, Y.-S.; Fu, W.-F. Copper(I) Complex Employed in Organic Light-Emitting Electrochemical Cells: Device and Spectra Shift. *Appl. Phys. Lett.* **2005**, *87*, No. 233512.
(9) Kalsani, V.; Schmittel, M.; Listorti, A.; Accorsi, G.; Armaroli, N. Novel Phenanthroline Ligands and Their Kinetically Locked Copper(I) Complexes with Unexpected Photophysical Properties. *Inorg. Chem.* **2006**, *45*, 2061−2067.
(10) Zhang, Q. S.; Zhou, Q. G.; Cheng, Y. X.; Wang, L. X.; Ma, D. G.; Jing, X. B.; Wang, F. S. Highly Efficient Electroluminescence from Green-Light-Emitting Electrochemical Cells Based on Cu^{I} Complexes. *Adv. Funct. Mater.* **2006**, *16*, 1203−1208.
(11) Sunesh, C. D.; Chandran, M.; Mathai, G.; Choe, Y. Highly Luminescent Yellow and Yellowish-Green Light-Emitting Electrochemical Cells Based on Cationic Iridium Complexes with Phenanthroline Based Ancillary Ligands. *Opt. Mater.* **2013**, *35*, 407−413.
(12) Sunesh, C. D.; Mathai, G.; Cho, Y. R.; Choe, Y. Optoelectronic Properties of Green and Yellow Light-Emitting Electrochemical Cells Based on Cationic Iridium Complexes. *Polyhedron* **2013**, *57*, 77−82.
(13) deMello, J. C.; Tessler, N.; Graham, S. C.; Friend, R. H. Ionic Space-Charge Effects in Polymer Light-Emitting Diodes. *Phys. Rev. B* **1998**, *57*, 12951−12963.

DOI: 10.1021/acsami.5b00875
ACS Appl. Mater. Interfaces 2015, 7, 7741−7751

(14) de Mello, J. C. Interfacial Feedback Dynamics in Polymer Light-Emitting Electrochemical Cells. *Phys. Rev. B* **2002**, *66*, No. 235210.
(15) Malliaras, G. G.; Slinker, J. D.; DeFranco, J. A.; Jaquith, M. J.; Silveira, W. R.; Zhong, Y.-W.; Moran-Mirabal, J. M.; Craighead, H. G.; Abruna, H. D.; Marohn, J. A. Operating Mechanism of Light-Emitting Electrochemical Cells. *Nat. Mater.* **2008**, *7*, 168−168.
(16) Smith, D. L. Steady State Model for Polymer Light-Emitting Electrochemical Cells. *J. Appl. Phys.* **1997**, *81*, 2869−2880.
(17) Lowry, M. S.; Bernhard, S. Synthetically Tailored Excited States: Phosphorescent, Cyclometalated Iridium(III) Complexes and Their Applications. *Chem.—Eur. J.* **2006**, *12*, 7970−7977.
(18) Bernhard, S.; Barron, J. A.; Houston, P. L.; Abruña, H. D.; Ruglovksy, J. L.; Gao, X.; Malliaras, G. G. Electroluminescence in Ruthenium(II) Complexes. *J. Am. Chem. Soc.* **2002**, *124*, 13624−13628.
(19) Buda, M.; Kalyuzhny, G.; Bard, A. J. Thin-Film Solid-State Electroluminescent Devices Based On Tris(2,2′-bipyridine)ruthenium-(II) Complexes. *J. Am. Chem. Soc.* **2002**, *124*, 6090−6098.
(20) Gao, F. G.; Bard, A. J. Solid-State Organic Light-Emitting Diodes Based on Tris(2,2′-bipyridine)ruthenium(II) Complexes. *J. Am. Chem. Soc.* **2000**, *122*, 7426−7427.
(21) Gao, F. G.; Bard, A. J. High-Brightness and Low-Voltage Light-Emitting Devices Based on Trischelated Ruthenium(II) and Tris(2,2′-bipyridine)osmium(II) Emitter Layers and Low Melting Point Alloy Cathode Contacts. *Chem. Mater.* **2002**, *14*, 3465−3470.
(22) Hosseini, A. R.; Koh, C. Y.; Slinker, J. D.; Flores-Torres, S.; Abruña, H. D.; Malliaras, G. G. Addition of a Phosphorescent Dopant in Electroluminescent Devices from Ionic Transition Metal Complexes. *Chem. Mater.* **2005**, *17*, 6114−6116.
(23) Rudmann, H.; Rubner, M. F. Single Layer Light-Emitting Devices with High Efficiency and Long Lifetime Based on Tris(2,2′-bipyridyl) Ruthenium(II) Hexafluorophosphate. *J. Appl. Phys.* **2001**, *90*, 4338−4345.
(24) Rudmann, H.; Shimada, S.; Rubner, M. F. Solid-State Light-Emitting Devices Based on the Tris-Chelated Ruthenium(II) Complex. 4. High-Efficiency Light-Emitting Devices Based on Derivatives of the Tris(2,2′-bipyridyl) Ruthenium(II) Complex. *J. Am. Chem. Soc.* **2002**, *124*, 4918−4921.
(25) Bernhard, S.; Gao, X.; Malliaras, G. G.; Abruña, H. D. Efficient Electroluminescent Devices Based on a Chelated Osmium(II) Complex. *Adv. Mater.* **2002**, *14*, 433−436.
(26) Felici, M.; Contreras-Carballada, P.; Smits, J. M. M.; Nolte, R. J. M.; Williams, R. M.; De Cola, L.; Feiters, M. C. Cationic Heteroleptic Cyclometalated Iridium^{III} Complexes Containing Phenyl-Triazole and Triazole-Pyridine Clicked Ligands. *Molecules* **2010**, *15*, 2039−2059.
(27) Slinker, J. D.; Gorodetsky, A. A.; Lowry, M. S.; Wang, J.; Parker, S.; Rohl, R.; Bernhard, S.; Malliaras, G. G. Efficient Yellow Electroluminescence from a Single Layer of a Cyclometalated Iridium Complex. *J. Am. Chem. Soc.* **2004**, *126*, 2763−2767.
(28) Sunesh, C. D.; Mathai, G.; Choe, Y. Green and Blue-Green Light-Emitting Electrochemical Cells Based on Cationic Iridium Complexes with 2-(4-Ethyl-2-pyridyl)-1*H*-imidazole Ancillary Ligand. *Org. Electron.* **2014**, *15*, 667−674.
(29) Sunesh, C. D.; Chandran, M.; Ok, S.; Choe, Y. Effect of Smaller Counter Anion, BF_4^-, on the Electroluminescent Properties of Cationic Iridium Complex Based Light-Emitting Electrochemical Cells. *Mol. Cryst. Liq. Cryst.* **2013**, *584*, 131−138.
(30) Hu, T.; He, L.; Duan, L.; Qiu, Y. Solid-State Light-Emitting Electrochemical Cells Based on Ionic Iridium(III) Complexes. *J. Mater. Chem.* **2012**, *22*, 4206−4215.
(31) Costa, R. D.; Ortí, E.; Bolink, H. J.; Monti, F.; Accorsi, G.; Armaroli, N. Luminescent Ionic Transition-Metal Complexes for Light-Emitting Electrochemical Cells. *Angew. Chem., Int. Ed.* **2012**, *51*, 8178−8211.
(32) Tamayo, A. B.; Garon, S.; Sajoto, T.; Djurovich, P. I.; Tsyba, I. M.; Bau, R.; Thompson, M. E. Cationic Bis-cyclometalated Iridium-(III) Diimine Complexes and Their Use in Efficient Blue, Green, and Red Electroluminescent Devices. *Inorg. Chem.* **2005**, *44*, 8723−8732.
(33) Sunesh, C. D.; Ok, S.; Mathai, G.; Choe, Y. Electroluminescent Properties of Yellow Light-Emitting Electrochemical Cells Based on a Cationic Iridium Complex and the Effect of Ionic Liquids Incorporation in an Active Layer. *Thin Solid Films* **2013**, *531*, 530−534.
(34) Su, H.-C.; Cheng, C.-Y. Recent Advances in Solid-State White Light-Emitting Electrochemical Cells. *Isr. J. Chem.* **2014**, *54*, 855−866.
(35) Wang, X.-j.; Tan, J.; Grozinger, K.; Betageri, R.; Kirrane, T.; Proudfoot, J. R. Practical Synthesis of 1,3-Diaryl-5-alkylpyrazoles by a Highly Regioselective N-arylation of 3,5-Disubstituted Pyrazoles with 4-Fluoronitrobenzene. *Tetrahedron Lett.* **2000**, *41*, 5321−5324.
(36) Lowry, M. S.; Hudson, W. R.; Pascal, R. A.; Bernhard, S. Accelerated Luminophore Discovery through Combinatorial Synthesis. *J. Am. Chem. Soc.* **2004**, *126*, 14129−14135.
(37) Sprouse, S.; King, K. A.; Spellane, P. J.; Watts, R. J. Photophysical Effects of Metal-Carbon σ bonds in Ortho-Metalated Complexes of Ir(III) and Rh(III). *J. Am. Chem. Soc.* **1984**, *106*, 6647−6653.
(38) Liu, Y.; Liu, M. S.; Jen, A. K. -Y. Synthesis and Characterization of a Novel and Highly Efficient Light-Emitting Polymer. *Acta Polym.* **1999**, *50*, 105−108.
(39) Hwang, S.-W.; Chen, Y. Synthesis and Electrochemical and Optical Properties of Novel Poly(Aryl Ether)s with Isolated Carbazole and *p*-Quaterphenyl Chromophores. *Macromolecules* **2001**, *34*, 2981−2986.
(40) Nonoyama, M. Benzo[*h*]Quinolin-10-yl-*N*-Iridium(III) Complexes. *Bull. Chem. Soc. Jpn.* **1974**, *47*, 767−768.
(41) Colombo, M. G.; Brunold, T. C.; Riedener, T.; Guedel, H. U.; Fortsch, M.; Buergi, H.-B. Facial Tris Cyclometalated Rhodium(3+) and Iridium(3+) Complexes: Their Synthesis, Structure, and Optical Spectroscopic Properties. *Inorg. Chem.* **1994**, *33*, 545−550.
(42) Frisch, M. J.; Trucks, G. W.; Schlegel, H. B.; Scuseria, G. E.; Robb, M. A.; Cheeseman, J. R.; Scalmani, G.; Barone, V.; Mennucci, B.; Petersson, G. A.; Nakatsuji, H.; Caricato, M.; Li, X.; Hratchian, H. P.; Izmaylov, A. F.; Bloino, J.; Zheng, G.; Sonnenberg, J. L.; Hada, M.; Ehara, M.; Toyota, K.; Fukuda, R.; Hasegawa, J.; Ishida, M.; Nakajima, T.; Honda, Y.; Kitao, O.; Nakai, H.; Vreven, T.; Montgomery, J. A., Jr.; Peralta, J. E.; Ogliaro, F.; Bearpark, M.; Heyd, J. J.; Brothers, E.; Kudin, K. N.; Staroverov, V. N.; Kobayashi, R.; Normand, J.; Raghavachari, K.; Rendell, A.; Burant, J. C.; Iyengar, S. S.; Tomasi, J.; Cossi, M.; Rega, N.; Millam, J. M.; Klene, M.; Knox, J. E.; Cross, J. B.; Bakken, V.; Adamo, C.; Jaramillo, J.; Gomperts, R.; Stratmann, R. E.; Yazyev, O.; Austin, A. J.; Cammi, R.; Pomelli, C.; Ochterski, J. W.; Martin, R. L.; Morokuma, K.; Zakrzewski, V. G.; Voth, G. A.; Salvador, P.; Dannenberg, J. J.; Dapprich, S.; Daniels, A. D.; Farkas, O.; Foresman, J. B.; Ortiz, J. V.; Cioslowski, J.; Fox, D. J. *Gaussian 09*, revision B.01; Gaussian, Inc.: Wallingford, CT, 2009.
(43) Becke, A. D. Density-Functional Thermochemistry. III. The Role of Exact Exchange. *J. Chem. Phys.* **1993**, *98*, 5648−5652.
(44) Becke, A. D. Density-Functional Thermochemistry. IV. A New Dynamical Correlation Functional and Implications for Exact-Exchange Mixing. *J. Chem. Phys.* **1996**, *104*, 1040−1046.
(45) Lee, C.; Yang, W.; Parr, R. G. Development of the Colle-Salvetti Correlation-Energy Formula into a Functional of the Electron Density. *Phys. Rev. B* **1988**, *37*, 785−789.
(46) Hay, P. J.; Wadt, W. R. Ab Initio Effective Core Potentials for Molecular Calculations. Potentials for the Transition Metal Atoms Sc to Hg. *J. Chem. Phys.* **1985**, *82*, 270−283.
(47) Hay, P. J.; Wadt, W. R. Ab Initio Effective Core Potentials for Molecular Calculations. Potentials for K to Au Including the Outermost Core Orbitals. *J. Chem. Phys.* **1985**, *82*, 299−310.
(48) Wadt, W. R.; Hay, P. J. Ab Initio Effective Core Potentials for Molecular Calculations. Potentials for Main Group Elements Na to Bi. *J. Chem. Phys.* **1985**, *82*, 284−298.
(49) Miertuš, S.; Scrocco, E.; Tomasi, J. Electrostatic Interaction of a Solute with a Continuum. A Direct Utilizaion of AB Initio Molecular Potentials for the Prevision of Solvent Effects. *Chem. Phys.* **1981**, *55*, 117−129.

DOI: 10.1021/acsami.5b00875
ACS Appl. Mater. Interfaces 2015, 7, 7741−7751

(50) Cossi, M.; Barone, V.; Cammi, R.; Tomasi, J. Ab Initio Study of Solvated Molecules: A New Implementation of the Polarizable Continuum Model. *Chem. Phys. Lett.* **1996**, *255*, 327−335.
(51) Chitumalla, R. K.; Gupta, K. S. V.; Malapaka, C.; Fallahpour, R.; Islam, A.; Han, L.; Kotamarthi, B.; Singh, S. P. Thiocyanate-Free Cyclometalated Ruthenium(II) Sensitizers for DSSC: A Combined Experimental and Theoretical Investigation. *Phys. Chem. Chem. Phys.* **2014**, *16*, 2630−2640.
(52) Edkins, R. M.; Fucke, K.; Peach, M. J. G.; Crawford, A. G.; Marder, T. B.; Beeby, A. Syntheses, Structures, and Comparison of the Photophysical Properties of Cyclometalated Iridium Complexes Containing the Isomeric 1- and 2-(2′-Pyridyl)pyrene Ligands. *Inorg. Chem.* **2013**, *52*, 9842−9860.
(53) Gu, X.; Fei, T.; Zhang, H.; Xu, H.; Yang, B.; Ma, Y.; Liu, X. Theoretical Studies of Blue-Emitting Iridium Complexes with Different Ancillary Ligands. *J. Phys. Chem. A* **2008**, *112*, 8387−8393.
(54) Cheng, J.-A.; Chen, C. H.; Liao, C. H. Solution-Processible Small Molecular Organic Light-Emitting Diode Material and Devices Based on the Substituted Aluminum Quinolate. *Chem. Mater.* **2004**, *16*, 2862−2868.
(55) He, L.; Qiao, J.; Duan, L.; Dong, G.; Zhang, D.; Wang, L.; Qiu, Y. Toward Highly Efficient Solid-State White Light-Emitting Electrochemical Cells: Blue-Green to Red Emitting Cationic Iridium Complexes with Imidazole-Type Ancillary Ligands. *Adv. Funct. Mater.* **2009**, *19*, 2950−2960.

DOI: 10.1021/acsami.5b00875
ACS Appl. Mater. Interfaces 2015, 7, 7741−7751